Distortion correction projection

Wide field-of-view (FOV) cameras with a short focal length, such as many trail and security cameras, can be particularly susceptible to distortion, making it important to account for during both camera pose estimation, and 3D to 2D point projection. A set of five coefficients describing radial distortion (k_1, k_2, k_3) and tangential distortion (p_1, p_2) are estimated during camera calibration and summarized by the distortion vector, d.

$$d = [k_1 \quad k_2 \quad p_1 \quad p_2 \quad k_3]. \tag{1}$$

Distortion coefficients are applied after transformation with the extrinsic matrix, **P,** and before projection with the intrinsic matrix **K.**

For additional details on implementation see the OpenCV documentation at:

https://docs.opencv.org/4.x/d9/d0c/group__calib3d.html

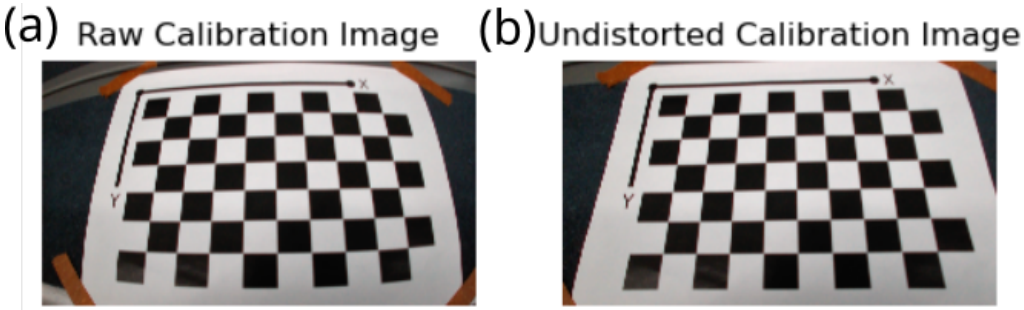

Figure S1: Example of a calibration image (a) before and (b) after correction with estimated distortion coefficients.

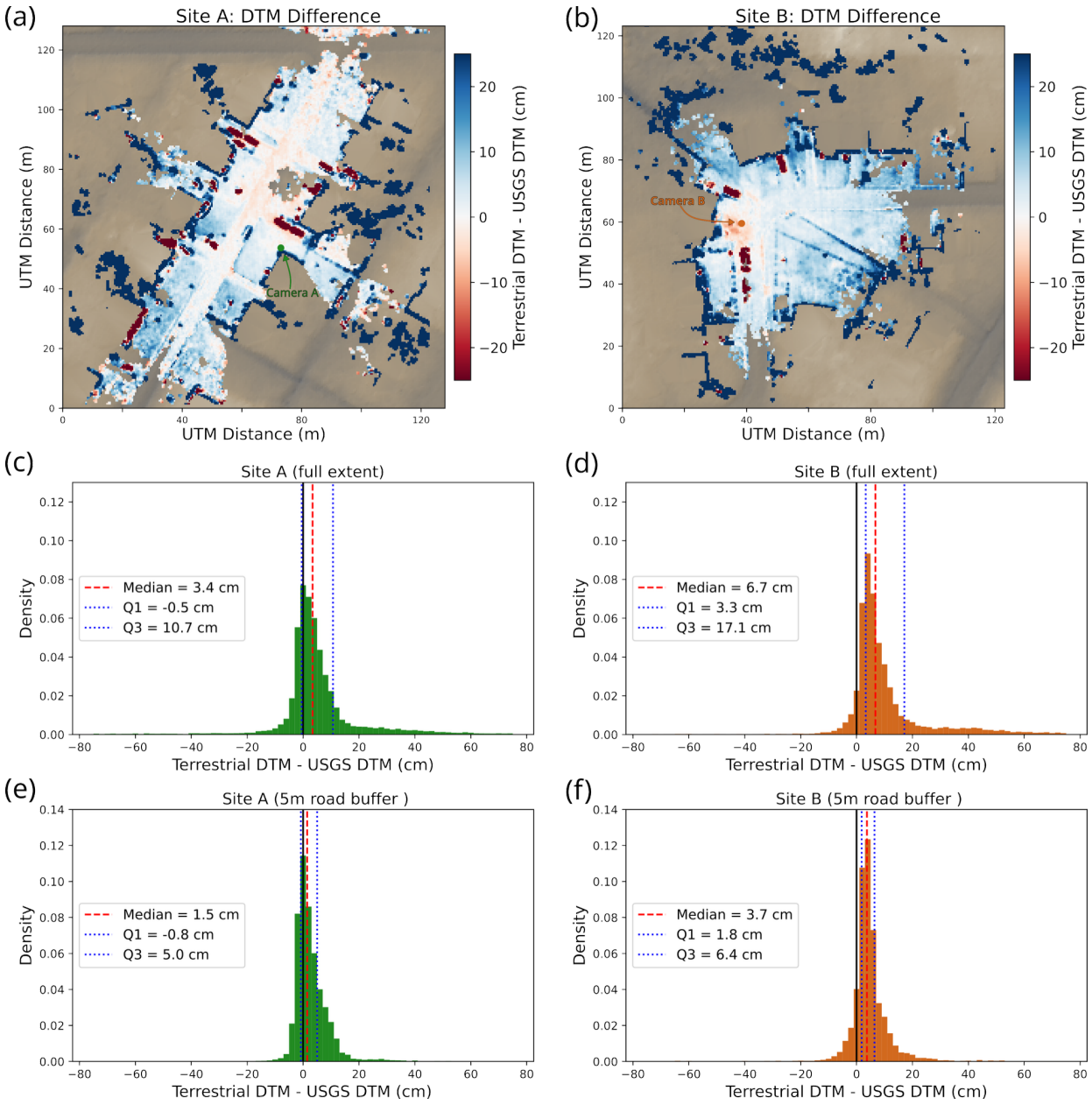

Figure S2: Elevation differences between the 0.5 m-resolution, georeferenced terrestrial lidar DTM (2023), and 0.5 m-resolution aerial USGS lidar DTM (2020) at (a) Site A and (a) Site B. Larger elevation differences are found around the edge of the survey extent, and where vehicles were present during the aerial scan (visible as red patches). However, differences are generally below 5 cm within 5 m of the road surface (c-f).

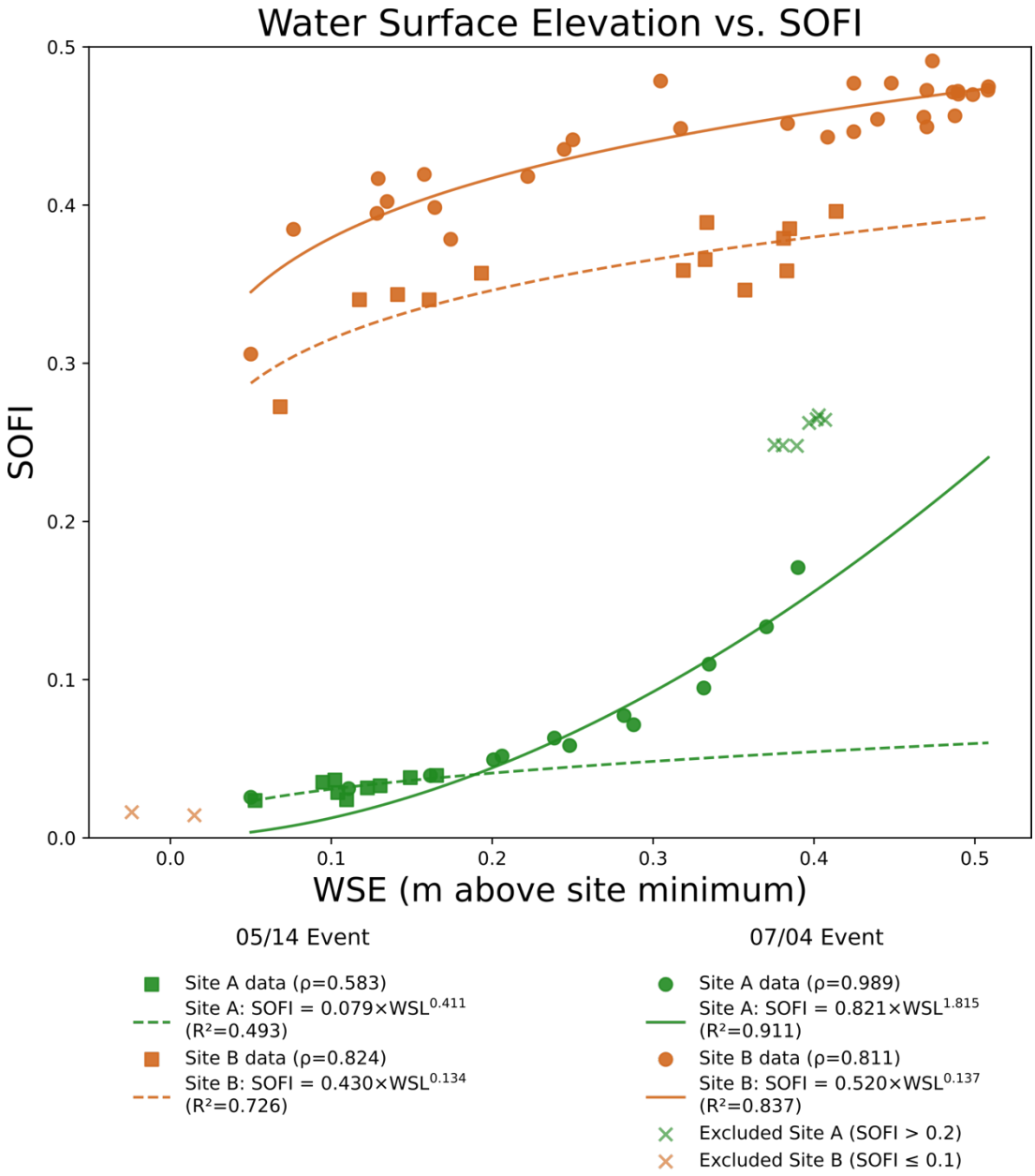

Figure S3: Fitted power law relationships between image derived Water Surface Elevation (*WSE*$_{90}$) and Static Observer Flooding Index *(SOFI)*. Water extension towards the camera (decreasing ground pixel size) produces a exponent > 1, such as the July event at Site A (green circles), while water extension away from the camera (increasing ground pixel size), produces an exponent < 1, such as at Site B (orange circles and squares). Images at Site A where flood extent passed the bottom of the image, and images of isolated puddles at Site B were excluded from fitting and are indicated by "X" symbols.

Camera pose estimation error evaluation

Table S1: Camera position (ΔC) and rotation errors *(R)* from the camera-lidar calibration test

	Ground control point estimated			*Static feature estimated*				*IMU*
	ΔC	R_{IMU}	$R_{initial}$	ΔC	R_{IMU}	R_{inital}	R_{GCP}	R_{inital}
Pose 1	0.06 m	2.11°	0.00°	0.07 m	2.14°	0.0°	0.17°	0.00°
Pose 2	0.06 m	1.63°	5.30°	0.10 m	1.65°	5.48°	0.11°	5.18°
Pose 3	0.04 m	1.52°	14.93°	0.17 m	1.62°	15.09°	0.27°	14.78°

For the case study events, camera pose was calculated based on available pre-existing static features rather than explicitly surveyed Ground Control Points (GCPs). A calibration test was performed to evaluate pose accuracy when using static features, compared to GCPs. The same model of trail-camera used in the study was mounted to a stable tripod, placed in an outdoor courtyard, and affixed with a 9-axis Inertial Measurement Unit (IMU) to record camera rotation, with a resolution of 0.01 degrees. With the tripod base stationary, images were taken from three different camera orientations. Within practical limits, camera roll and yaw were kept constant, only adjusting camera pitch over a range of 15 degrees. Three lidar scans were collected simultaneously with photo collection. 21 reflective targets were deployed throughout the image field-of-view as ground control points. 22 static features including window corners, fence posts, and utility poles were also identified. Three lidar scans were collected of the scene. Following camera calibration, both GCPs and static features were labeled in the images and point cloud. Three rotation-translation matrices (**P**) were calculated for each camera pose. Our ground truth pose was calculated from IMU measured *X, Y, Z* rotation, and point cloud labeled camera location. The second was estimated from our labeled GCPs using RANSAC optimized EPnP (Lepetit et al., 2009). The third was estimated from our labeled static features in the same manner.

Position error is characterized by the absolute distance between labeled and recovered *X, Y, Z* camera locations (ΔC). Absolute camera rotation error (R_{IMU}) was characterized by the magnitude of rotation between separating the IMU measurements and the estimated rotation matrix. Similarly, relative rotation error ($R_{initial}$) was characterized by the magnitude of rotation from the initial camera position, Pose 1, as calculated by each method. Error in camera location was overall slightly higher when only using static features, but in all cases remained less than 20 cm. Absolute rotation errors were similar between approaches, and all below 2.5°. Rotations relative to the initial camera pose are more consistent, with an average difference of 0.14° and 0.31° from the IMU for GCP and static feature estimates respectively, suggesting a potential offset between the IMUs calibration and the point cloud. This gives us some expectation for the camera pose accuracy achievable with our camera and lidar equipment, in outdoor conditions similar to those of our flood monitoring stations.